第 35 卷第 2 期
2019 年 2 月

无 机 化 学 学 报
CHINESE JOURNAL OF INORGANIC CHEMISTRY

Vol.35 No.2
351-360

一个对 2,4,6-三硝基苯酚和 Fe^{3+}离子具有双重荧光传感行为的层状镉(Ⅱ)-有机配位聚合物

石静静 徐 珊 李 娜 王修光 赵小军* 杨恩翠*

(天津师范大学化学学院,无机–有机杂化功能材料化学教育部重点实验室,
天津市功能分子结构与性能重点实验室,天津 300387)

摘要: 通过水热法合成了一个由三连接的 2,3-喹啉二甲酸桥联扭曲的 Cd^{2+}八面体形成的二维层状配位聚合物$[Cd(QDA)]_n$ (**1**)。该配合物发射出较强的蓝色荧光并具有很高的热稳定性和化学稳定性。更为重要的是,该配合物在乙醇分散体系中可快速识别痕量的 2,4,6-三硝基苯酚和 Fe^{3+}离子,其对 2,4,6-三硝基苯酚的淬灭常数(K_{sv})和检测限(LOD)分别为 6.61×10^4 L·mol^{-1} 和 0.83 μmol·L^{-1},对 Fe^{3+}离子的淬灭常数和检测限分别为 1.74×10^4 L·mol^{-1} 和 2.70 μmol·L^{-1}。

关键词: 配位聚合物; 2,3-喹啉二甲酸; 晶体结构; 淬灭常数; 荧光传感
中图分类号: O614.24+2 **文献标识码**: A **文章编号**: 1001-4861(2019)02-0351-10
DOI: 10.11862/CJIC.2019.045

A Layered Cd(Ⅱ)-Organic Coordination Polymer Exhibiting Dual-Responsive Sensing Towards 2,4,6-Trinitrophenol and Fe^{3+}

SHI Jing-Jing XU Shan LI Na WANG Xiu-Guang ZHAO Xiao-Jun* YANG En-Cui*

(*College of Chemistry, Tianjin Normal University, Key Laboratory of Inorganic-Organic Hybrid Functional Material Chemistry, Ministry of Education, Tianjin Key Laboratory of Structure and Performance for Functional Molecules, Tianjin* 300387, *China*)

Abstract: A layered coordination polymer $[Cd(QDA)]_n$ (**1**) with distorted Cd^{2+} octahedron extended by three-connected 2,3-quinoline dicarboxylate linkers was hydrothermally synthesized, exhibiting intense blue fluorescence and highly thermal and chemical stability. More interestingly, the complex dispersed in ethanol can quickly probe the trace amounts of 2,4,6-trinitrophenol ($K_{sv}=6.61\times10^4$ L·mol^{-1}, LOD=0.83 μmol·L^{-1}) and Fe^{3+} ($K_{sv}=1.74\times10^4$ L·mol^{-1}, LOD=2.70 μmol·L^{-1}) through fluorescence quenching with high quenching constants (K_{sv}) and low limits of detection (LOD). CCDC: 1869887.

Keywords: coordination polymer; 2,3-quinoline dicarboxylic acid; crystal structure; quenching constant; fluorescence sensing

0 Introduction

Coordination polymers (CPs) constructed from diverse organic connectors and inorganic metal ions or metal clusters have attracted intense interest due to their intriguing structures and wide applications in gas adsorption and storage, catalysis, fluorescent sensing, drug delivery and so on. Due to the facile fabrication, good chemical and environmental stability as well as tailorable crystalline structures[1], luminescent CPs with d^{10} configuration of transition metal ions have been recently designed and prepared by varying the organic ligands with different electron-rich skeletons, such as 3,3′,5,5′-biphenyltetracarboxylate, N^1-(4-(1*H*-

收稿日期:2018-10-02。收修改稿日期:2018-12-05。
国家自然科学基金(No.21671149,21571140,21531005)和天津市高等学校创新团队培养计划(No.TD13-5074)资助。
*通信联系人。E-mail:encui_yang@163.com,xiaojun_zhao15@163.com

1,2,4-triazole-1-yl)benzyl)-N^1-(2-aminoethyl)ethane-1,2-diamine, 1,4-naphthalene dicarboxylate, 9-(4-carboxy-phenyl)-9*H*-carbazoly-3,6-dicarboxylate[2-4]. These interesting CPs have been extensively used as functional sensors to detect heavy metal ions, anions and small molecules to resolve the increasingly environmental concerns and pollution crises[2,5-6]. Undoubtedly, various factors including the emission intensity, decay lifetime, quantum yield as well as charge transfer efficiency have been known to significantly govern the selectivity and sensitivity of the sensing ability, which can be technically manipulated by the subtle choice of the fluorescent metal ions and organic connectors with different π-conjugated backbones and functional coordination groups[7-8].

Acting as one of important ingredients of both the harmful explosives and the essentially raw materials of chemical industries, nitroaromatic compounds, such as 2,4,6-trinitrophenol (PA), 4-methylnitrobenzene (4-NT), 2,4-dinitrotoluene (2,4-DNT), 1,4-dinitrobenzene (1,4-DNB) and 1,3-dinitrobenzene (1,3-DNB), have been one of the major issues involving national security and environmental protection. Among these frequently used nitroaromatic compounds, PA with the strongest explosive capacity has been extensively applied in the dye, pesticide and pharmaceuticals industry and recognized as a toxic source responsible for the seriously environmental pollution. The prolonged abuse of PA has already resulted in severe threats to the health of the human beings and mammalian, such as anemia, carcinogenicity, abnormal liver function, neurological damage, skin irritation and mutagenic activity[3,9-10]. Additionally, inorganic ion Fe^{3+} is one of the most common and important elements in the living biological systems, and plays a crucial role in a variety of vital cell functions such as cell metabolism, electron transfer enzyme catalysis, oxygen transport and syntheses of DNA and RNA. However, high residue level of Fe^{3+} can also destroy the normal functions of immune and enzyme systems, leading consequently to various health hazardous symptoms[11-13]. Therefore, it is significantly important to explore highly efficient luminescent sensors to quickly probe PA and Fe^{3+} in aqueous medium.

Herein, to investigate the fluorescent sensing behavior of the transition metal-based CPs, a facile self-assemble reaction of luminescent Cd^{2+} ion with aromatic 2,3-quinoline dicarboxylic acid (H_2QDA) was hydrothermally performed. As a result, a highly stable two-dimensional (2D) layered CP with the formula of $[Cd(QDA)]_n$ (**1**) was successfully obtained, which can selectively and sensitively discriminate the trace amounts of PA and Fe^{3+} through fluorescence quenching. In this context, hydrothermal synthesis, crystal structure, thermal and chemical stability, as well as sensing responses of **1** towards nitroaromatic coumpounds and inorganic metal ions were discussed in more details.

1 Experimental

1.1 Materials and physical measurements

All initial reagents were commercially purchased from Heowns Biochem LLC and used without any further purification. Doubly deionized water was used for the conventional synthesis. Elemental analyses for C, H and N were carried out with a CE-440 (Leeman-Labs) analyzer. Fourier transform (FT) IR spectra (KBr pellets) was recorded on an Avatar-370 (Nicolet) spectrometer in a range of 400~4 000 cm^{-1}. Thermogravimetric analysis (TGA) experiment was recorded on a Shimadzu simultaneous DTG-60A compositional analysis instrument from room temperature to 800 ℃ under a nitrogen flow at a heating rate of 5 ℃·min^{-1}. Powder X-ray diffraction (PXRD) patterns were collected from 5° to 50° with a step of 0.01° in 2θ on a Bruker D8 advance X-ray diffractometer with Cu Kα radiation (λ=0.154 056 nm) at 40 kV and 40 mA. A simulated PXRD pattern was calculated using single-crystal X-ray diffraction data and processed by the free Mercury v1.4 program downloaded from the Cambridge Crystallographic Data Center. Emission and excitation spectra were investigated on a Fluorolog-3 fluorescence spectrophotometer from Horiba Jobin Yvon and FLS1000 spectrometer from Edinburgh. UV-Vis absorption spectra was performed

with a Shimadzu UV-2700 spectrophotometer. Optical images of the sample were obtained by a Leica DM6 B upright digital research microscopes from Leica microsystems.

1.2 Synthesis of [Cd(QDA)]$_n$ (1)

A mixture of $Cd(NO_3)_2\cdot 4H_2O$ (30.8 mg, 0.1 mmol) and H_2QDA (21.7 mg, 0.1 mmol) was dissolved in doubly deionized water (8.0 mL). The resulting mixture was then sealed into a 23.0 mL Teflon-lined autoclave and heated at 80 ℃ for 96 hours. After the mixture was slowly cooled to room temperature at a rate of 1.5 ℃·h^{-1}, colorless block-shaped crystals suitable for single-crystal X-ray diffraction were obtained directly, manually separated and dried in air. Yield: 90% (based on H_2QDA). Elemental analysis Calcd. for $C_{11}H_5CdNO_4$(%): C, 40.33; H, 1.54; N, 4.28. Found(%): C, 40.31; H, 1.55; N, 4.29. FT-IR (KBr, cm^{-1}): 3 056 (w), 1 639 (s), 1 546 (s), 1 454(s),1 390 (s), 1 302 (m), 1 144 (w), 876 (w), 816 (w), 773(w), 736(w), 671 (w), 615(w), 474(w), 426(w).

1.3 X-ray crystallography

Diffraction intensity for **1** was collected at 296 K on a Bruker APEX-Ⅱ CCD diffractometer equipped with graphite-monochromatic Mo $K\alpha$ radiation with a radiation wavelength of 0.071 073 nm by using the φ-ω scan technique. There was no evidence of crystal decay during data collection. Semi-empirical multi-scan absorption corrections were applied using SADABS[14], and the program SAINT[15] was used for the integration of the diffraction profiles. The structure of **1** was solved by direct methods and refined using the full-matrix least-squares techniques using the SHELXL-97 and SHELXS-97 programs[16]. All non-hydrogen atoms were refined with anisotropic thermal refinement, and the carbon-bound hydrogen atoms were introduced at calculated positions. The structure-refinement parameters and the selected bond lengths and angles were listed in Table 1 and Table 2, respectively.

CCDC: 1869887.

Table 1　Crystal data and structure refinement for 1

Empirical formula	$C_{11}H_5CdNO_4$	D_c / (g·cm^{-3})	2.296
Formula weight	327.56	h, k, l	−8~9, −6~6, −14~12
Crystal size / mm	0.22×0.21×0.18	F(000)	316
Crystal system	Monoclinic	μ / mm^{-1}	2.305
Space group	$P2_1/c$	Reflection collected, unique	2 717, 1 743
a / nm	0.785 6(3)	R_{int}	0.033 1
b / nm	0.528 4(2)	Data, restraint, parameter	1 743, 107, 154
c / nm	11.655(5)	R_1[a], wR_2[b] [$I>2\sigma(I)$]	0.055 8, 0.130 1
β / (°)	101.714(7)	R_1, wR_2 (all data)	0.067 4, 0.137 0
V / nm^3	0.473 7(3)	GOF on F^2	1.045
Z	2	$(\Delta\rho)_{max}$, $(\Delta\rho)_{min}$ / (e·nm^{-3})	2 819, −1 190

[a] $R_1=\sum(||F_o|-|F_c||)/\sum|F_o|$; [b] $wR_2=[\sum w(|F_o|^2-|F_c|^2)^2/\sum w(F_o^2)^2]^{1/2}$.

Table 2　Selected bond lengths (nm) and angles (°) for 1

Cd(1)-O(1)	0.229 6(9)	Cd(1)-O(2)	0.242 1(10)	Cd(1)-O(2)^{iii}	0.230 9(10)
Cd(1)-O(3)^{i}	0.223 5(10)	Cd(1)-O(4)^{ii}	0.224 0(10)	Cd(1)-N(1)^{ii}	0.242 2(12)
O(1)-Cd(1)-O(2)	55.2(5)	O(1)-Cd(1)-O(2)^{iii}	94.6(5)	O(1)-Cd(1)-O(3)^{i}	134.8(6)
O(1)-Cd(1)-N(1)^{ii}	94.7(4)	O(1)-Cd(1)-O(4)^{ii}	126.9(5)	O(2)-Cd(1)-O(2)^{iii}	82.0(2)
O(2)-Cd(1)-O(3)^{i}	83.2(4)	O(2)-Cd(1)-N(1)^{ii}	117.0(4)	O(2)^{iii}-Cd(1)-O(3)^{i}	96.2(4)
O(2)^{iii}-Cd(1)-O(4)^{ii}	89.4(4)	O(3)^{i}-Cd(1)-N(1)^{ii}	88.9(4)	O(3)^{i}-Cd(1)-O(4)^{ii}	97.0(4)
O(4)^{ii}-Cd(1)-N(1)^{ii}	71.7(4)				

Symmetry codes: [i] $-x$, $y-1/2$, $-z$; [ii] $x-1$, y, z; [iii] $-x$, $y+1/2$, $-z$.

1.4 Luminescent sensing experiments

Finely-ground crystalline powder of **1** (6.0 mg) was respectively immersed in the selected solvent (30.0 mL) including ethanol, methanol, water, *N*,*N*-dimethylformamide (DMF) and acetonitrile. Then, the resulting mixture was treated by ultrasonication for 5 min to form a stable dispersion prior to the fluorescence measurement. The sensing experiment was carried out by injecting 20 μL nitroaromatic compound (PA, 4-NT, 2,4-DNT, 1,4-DNB and 1,3-DNB, 10 mmol·L^{-1}) or 300 μL metal ion (K^+, Na^+, Ni^{2+}, Ca^{2+}, Mn^{2+}, Zn^{2+}, Ba^{2+} and Fe^{3+}, 5.0 mmol·L^{-1}) into the dispersion of **1**-ethanol (0.2 mg·mL^{-1}, 3.0 mL). The resulting mixture was treated by ultrasonication for 5 min before the emission measurement. Fluorescence titration experiments were carried out by gradually injecting PA (10 mmol·L^{-1}) or Fe^{3+} solution (5.0 mmol·L^{-1}) into the suspension of 1 in ethanol (0.2 mg·mL^{-1}, 3.0 mL) and fluorescence intensity of the resulting stable emulsion was monitored.

2 Results and discussion

2.1 Synthesis and IR spectrum

Hydrothermal reaction of H_2QDA with hydrated $Cd(NO_3)_2$ at 80 ℃ successfully afforded well-shaped single-crystals of **1** with a satisfactory yield. Reaction temperature was found to play more important roles on the yield and size of the resultant product. In the IR spectra of **1**, a weak absorption at 3 056 cm^{-1} is assigned to the stretching vibration of aromatic C-H from quinolyl ring. As compared with the free organic acid, the absence of a characteristic band at 1 691 cm^{-1} in **1** indicates the deprotonation of the carboxylic group in H_2QDA. Correspondingly, the asymmetric and symmetric stretching bands for the carboxylate moieties are located at 1 639, 1 546, 1 454 and 1 390 cm^{-1}. Thus, the IR data of **1** is consistent with the results of the single-crystal structural analysis.

2.2 Crystal structure of 1

Single-crystal X-ray structural analysis reveals that **1** crystallizes in the monoclinic space group $P2_1/c$ (Table 1), exhibiting a fishbone-shaped 2D coordination layer with the slightly distorted Cd^{2+} octahedra extended by three-connected QDA^{2-} linkers. The asymmetric unit of **1** contains one Cd^{2+} ion and one doubly deprotonated QDA^{2-} anion for charge compensation. As shown in Fig.1a, the unique Cd^{2+} site in **1** is six-coordinated in NO_5 donor set, adopting a slightly distorted octahedral coordination geometry. The equatorial plane of Cd^{2+} octahedron are occupied by four carboxylate O donors from three crystallographically identical QDA^{2-} anions. By contrast, the two axial sites are respectively furnished by one quinolyl N and one carboxylate O donors from two individual QDA^{2-} ligands. The equatorial Cd-O distances are slightly shorter by 0.01 nm than those in the axial positions (Table 2), suggesting an axially elongated octahedron. The H_2QDA ligand in **1** is in a doubly deprotonated form, behaving as a bridging connector to extend Cd^{2+} ion through a pendentate (four carboxylate O and one quinolyl N donors) coordination mode (Fig.S1).

As illustrated in Fig.1b, the QDA^{2-} ligand acts as a three-connected linker to bridge the adjacent Cd^{2+} ions through two carboxylate moieties, leading to a fishbone-shaped 2D layer with the intralayer $Cd^{2+}\cdots Cd^{2+}$ distances of 0.443 67(10) and 0.561 08(17) nm

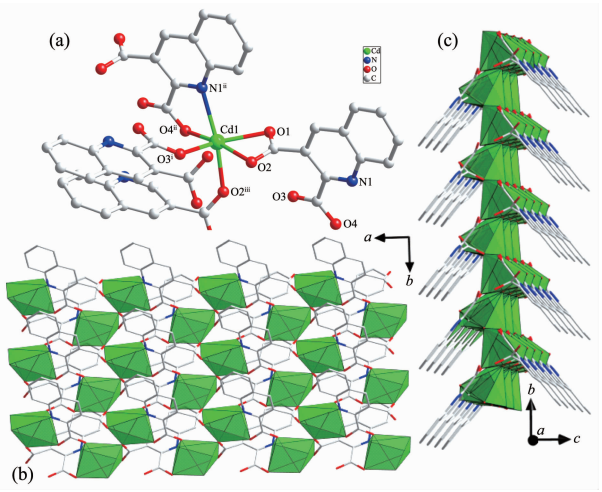

H atoms are omitted for clarity; Symmetry codes: [i] $-x, y-1/2, -z$; [ii] $x-1, y, z$; [iii] $-x, y+1/2, -z$

Fig.1 (a) Local coordination environments of Cd^{2+} ion in **1**; (b) 2D layered structure of **1** viewed vertically to crystallographic *ab* plane; (c) Fishbone-shaped layered structure of **1** viewed vertically to crystallographic *bc* plane

separated by single-atom bridging and bidentate bridging carboxylate groups (Fig.1b and 1c). Due to the exterior alignment of the hydrophobic phenyl moiety of QDA^{2-} ligands, the individual 2D sheets of **1** are isolated with each other without any weak interlayer non-covalent interaction. The interlayer $Cd^{2+}\cdots Cd^{2+}$ separation is 1.16 nm (Fig.S2), which is much longer than the intralayer intermetallic distances.

2.3 PXRD and TG curve of 1

The PXRD pattern of the as-prepared sample was well consistent with the simulated one (Fig.2), implying the high pure-phase of **1** and the structural consistency of the as-synthesized sample with the single-crystal data. The TG curve of **1** had no obvious weight-loss below 400 ℃ (Fig.S3), revealing highly thermal stability of **1**. Upon further heating, a rapid weight-loss stage for the collapse of the layered framework was observed beyond 400 ℃. The PXRD pattern of **1** after heating at 350 ℃ for five hours was the same as that of the as-prepared sample, further confirming the TG result. Chemical stability of **1** was evaluated by soaking the ground sample in aqueous solutions with different pH values for 24 hours. The PXRD patterns of **1** recovered from different water systems were the same as that of the simulated one (Fig.2), suggesting that **1** has highly chemical stability in a wide pH range. The solvent stability of **1** was also checked by the well matched PXRD patterns of **1** before and after soaking in a given medium such as ethanol, methanol, water, acetonitrile and DMF (Fig.2).

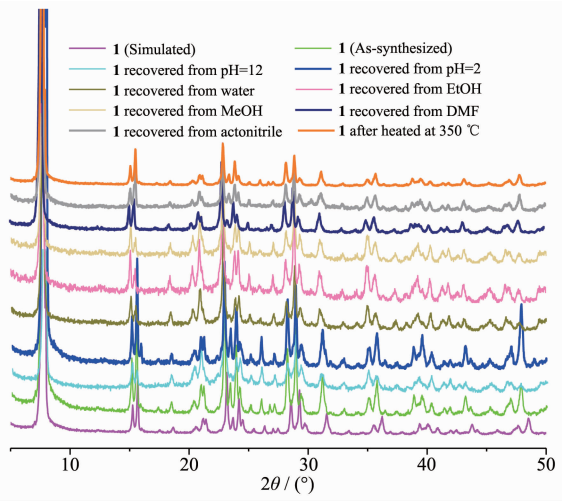

Fig.2 PXRD patterns of **1** towards various external stimulus

2.4 Photoluminescence properties

Excitation and emission spectra of **1** and free H_2QDA were recorded in the solid-state at room temperature. Upon excitation at 348 nm, complex **1** displayed an intense emission at 364 nm and a weak abroad fluorescence centered at 522 nm (Fig.3). The intense emission of **1** has a bright blue light (Inset in Fig.3). Under the same measuring conditions, H_2QDA ligand exhibited a broad emission centered at 390 nm upon excitation at 350 nm due to the π-π^* and/or n-π^* electron transitions from benzenyl and pyridyl rings of ligands[17]. Weak dark green fluorescence of the H_2QDA ligand can also be observed by naked eyes (Inset in Fig.3). Apparently, the intraligand charge transfer of **1** blue-shifted by 26 nm with apparently enhanced intensity as compared with that of free H_2QDA ligand, which is due to the coordination behavior of organic ligand with metal ion.

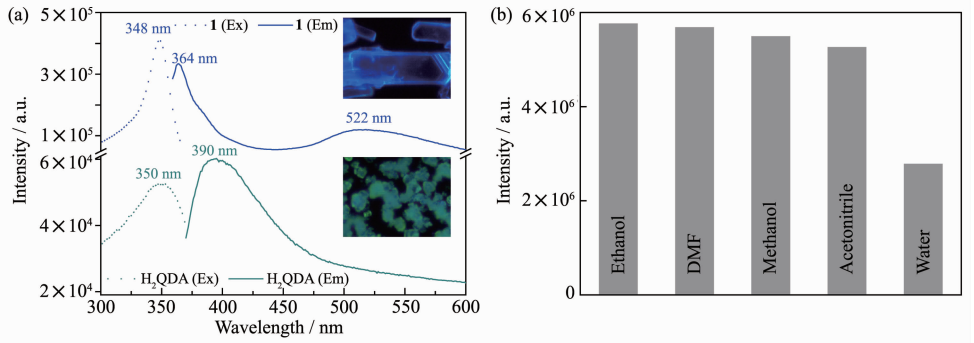

Inset: photographs of H_2QDA and **1** through fluorescence microscope

Fig.3 (a) Excitation and emission spectra of **1** and H_2QDA in the solid-state measured at room temperature; (b) Luminescence intensity of **1** at 364 nm in different media

Notably, the intensity of **1** at 364 nm was five times stronger than that of H_2QDA ligand at 390 nm, and the relatively weak emission may restrict significantly the applications of H_2QDA as luminescence probe.

2.5 Probing for nitroaromatic compounds

Intense emission of **1** with bulky conjugated chromophore group can potentially provide excellent sensing performance towards different analytes. The optimized medium for **1** was firstly investigated before the fluorescent responses. Because the organic ligand in the ligand-based emission systems can absorb the excitation energy to give the corresponding fluorescence, which can induce energy transfer between the organic ligand and solvent and cause the quenching of the fluorescence[18]. As a result, the positions of the emission band of **1** dispersed in various solvents were the same as those in the solid-state due to the insignificant solvent effect. By contrast, the emission intensity of **1** decreased slightly in different media, and followed the sequence: $I_{ethanol} > I_{DMF} > I_{MeOH} > I_{acetonitrile} > I_{water}$ (Fig.3b). Thus, ethanol system with the strongest intensity was selected as the best medium for the sensing investigations of **1**.

In the presence of nitroaromatic compounds, the emission intensity of **1** at 364 nm decreased to some different degree (Fig.4a), in which a drastic quenching

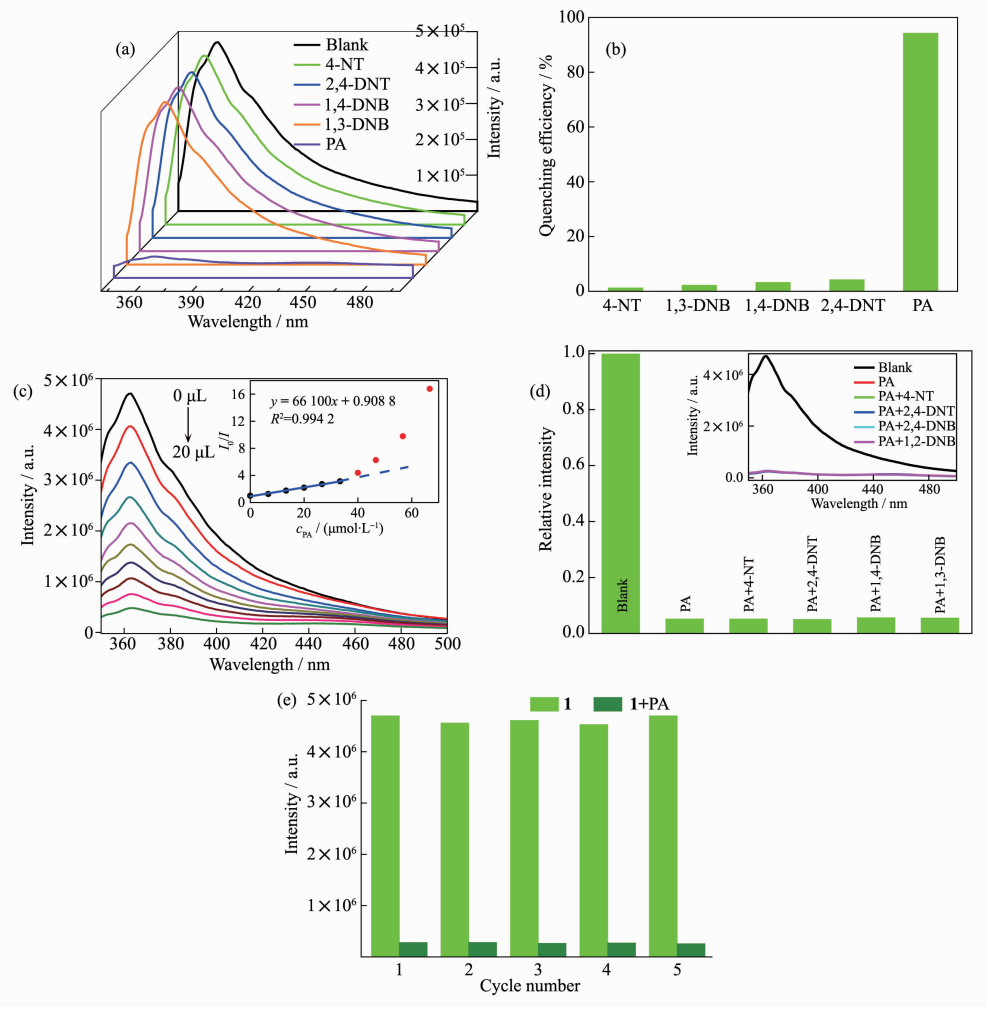

Inset in (c): plot of I_0/I vs c_{PA} for **1**, straight line represents the best fit to Stern-Volmer equation

Fig.4 (a) Emission spectra of **1** dispersed in ethanol in the absence and presence of selected nitroaromatic compounds upon excitation at 335 nm; (b) Quenching efficiency of **1** by different nitroaromatic compounds; (c) Fluorescence titration of **1** upon incremental addition of PA; (d) Fluorescent response of **1** towards 66.7 μmol·L^{-1} PA and a mixture of competing nitroaromatic compounds (66.7 μmol·L^{-1}) and 66.7 μmol·L^{-1} PA; (e) Recycle tests of **1** implemented with 66.7 μmol·L^{-1} of PA solution

effect was observed by PA. The quenching efficiency of **1** by PA was as high as 90.6%, and the quenching efficiency of **1** by other selected nitroaromatic compounds varied only between 1% and 4% (Fig.4b). Therefore, **1** dispersed in ethanol can highly selective sensing PA. To quantitatively evaluate the quenching constant, fluorescence titration experiment of **1** was implemented by gradual addition of PA into the suspension of **1** in ethanol. As shown in Fig.4c, the intensity of **1** at 364 nm progressively decreased with the gradual increment of PA solution. Once the concentration of PA increased up to 66.6 μmol·L^{-1}, the fluorescence intensity of **1** was almost completely quenched. The plot of I_0/I vs c_{PA} was nearly linear at low PA concentrations in a range of 0~33.3 μmol·L^{-1}, resulting from the static quenching[4]. Subsequently, the curve of I_0/I vs c_{PA} deviated from linearity and bended upwards with a steep increase, which is due to the energy-transfer and/or self-absorption process[4]. The linear portion of the quenching curve can be well fitted to the Stern-Volmer (S-V) equation: $I_0/I=1+K_{SV}c_{PA}$, where I_0 and I are the luminescence intensity before and after addition of PA, respectively, and K_{SV} is the quenching constant. The results afforded the simple linear equation of y=66 100x+0.908 8 with the correlation coefficient R^2=0.994 2 (Fig.4d), meaning that the quenching constant of **1** by PA was 6.61×10^4 L·mol^{-1}. Acting as one of important parameters for describing the sensing ability, the limit of detection (LOD) can be calculated by $3\sigma/k$, in which σ is the standard error for several independently parallel experiments and k is slope extracted from the linear regression of I vs c_{PA}. The LOD of **1** towards PA is calculated to be 0.83 μmol·L^{-1} (Table S1).

Anti-interference experiments of other nitroaromatic compounds have been done to estimate the sensing sensitivity of **1** towards PA. As illustrated in Fig.4e, the intensity of **1** at 364 nm in the presence of PA was almost the same as those of **1** in the presence of PA and one of the other nitroaromatic compounds, suggesting that the co-existence of the second nitroaromatic compound insignificantly influences the recognition behavior of **1** to PA.

2.6 Sensing for Fe^{3+}

To explore the multiple fluorescent-responsive ability, the sensing of **1** to a series of inorganic metal ions were carried out in ethanol system. As shown in Fig.5a and Fig.5b, the intensity of **1** at 364 nm was quenched to some different extent by the selected metal ions with the most pronounced quenching effect observed by Fe^{3+}. Thus, **1** can high-selectively probe Fe^{3+}. The quenching constant of **1** by Fe^{3+} was quantitatively calculated by the fluorescence titration experiment (Fig.5c). Obviously, the emission intensity of **1** depended heavily on the concentration of Fe^{3+}. In the low concentrations ranging from 0 to 200.0 μmol·L^{-1}, the plot of I_0/I vs $c_{Fe^{3+}}$ was linear due to the static quenching[4], obeying the S-V equation well with K_{sv}= 17 400 and R^2=0.997 7 (Fig.5d). Once the concentration of Fe^{3+} was beyond 200 μmol·L^{-1}, the plot of I_0/I vs $c_{Fe^{3+}}$ bended upwards resulting from dynamic quenching[4]. The quenching efficiency of **1** by Fe^{3+} was up 92.0% when the concentration of Fe^{3+} was 300 μmol·L^{-1}. The LOD of **1** towards Fe^{3+} was further estimated to be 2.70 μmol·L^{-1} (Table S1).

The emission intensity of **1** at 364 nm in the presence of Fe^{3+} was nearly identical with those of the mixture containing Fe^{3+} and one of the inorganic ion of interest (Fig.5e). The similar quenching behavior of **1** in various different metal ions indicates that **1** can high-selectively probe Fe^{3+} even in the presence of other interference substances.

2.7 Regeneration and recyclability

Regeneration and recyclability are important indicators for the practical applications of the fluorescent probes. The dispersions of **1** after sensing PA and Fe^{3+} were centrifuged, and the solid powers were collected and washed with water three times. The PXRD pattern and the florescence intensity of the recovered **1** were almost the same as those before the sensing experiments, suggesting that **1** can maintain the stability of skeleton during the repeated identification experiments. Moreover, the intensity at 364 nm and the quenching efficiency of **1** have not been significantly altered after five cycles (Fig.4e and

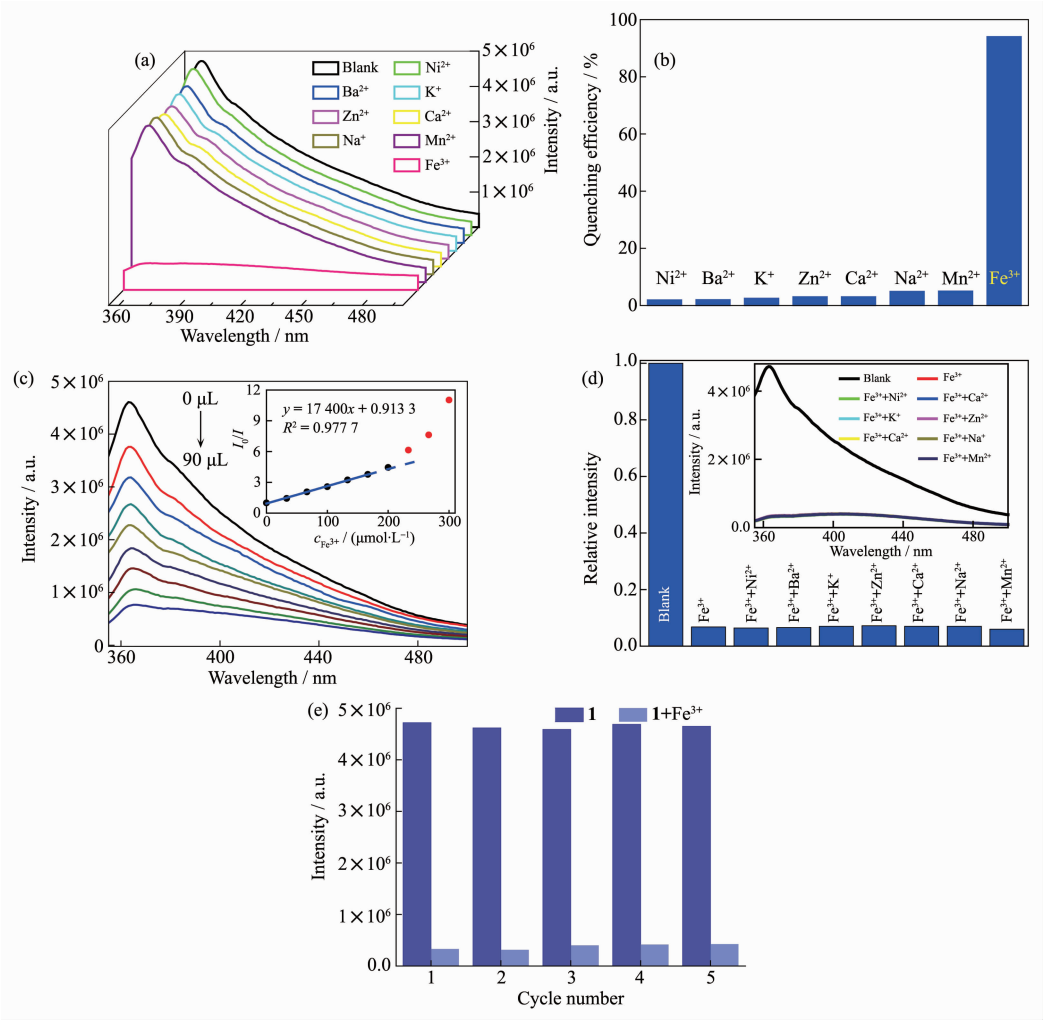

Inset in (c): plot of I_0/I vs $c_{Fe^{3+}}$ for **1**, straight line represents the best fit to S-V equation

Fig.5 (a) Emission spectra of **1** dispersed in ethanol in the absence and presence of selected metal ions upon excitation at 335 nm; (b) Quenching efficiency of **1** by different metal ions; (c) Fluorescence titration of **1** upon incremental addition of Fe^{3+}; (d) Fluorescent responses of **1** towards 300.0 μmol·L^{-1} Fe^{3+} and a mixture containing one interference ion (300.0 μmol·L^{-1}) and 300.0 μmol·L^{-1} Fe^{3+}; (e) Recyclability tests of **1** implemented with 300.0 μmol·L^{-1} Fe^{3+} in ethanol solution

5e), implying that **1** has high recyclability and regeneration ability and can be long-term reused for the detection of PA and Fe^{3+} without significant loss of recognition ability.

2.8 Mechanism for sensing PA and Fe^{3+}

To better understand the mechanism of the fluorescence quenching effect of **1** by PA and Fe^{3+}, PXRD, UV-Vis absorption and fluorescent lifetime experiments have been done, respectively. Firstly, the PXRD patterns of **1** before and after sensing experiments agree well with each other (Fig.S4), indicating that the retention of framework of **1** after sensing experiments. At the same time, the fluorescence lifetime of **1** in the presence of PA and Fe^{3+} are almost unchanged compared with that of **1** dispersed in ethanol (Fig.6 and Table S2), proving that no interactions are observed between PA or Fe^{3+} and **1**. Therefore, the absorption competition of the light source energy between the analyte and ligand in **1** may be the key factor for high selective detection of PA or Fe^{3+}. As shown in Fig.7, the UV-Vis absorption spectra of PA and Fe^{3+} had significantly absorption from 350 to 400 nm, showing a maximum spectral overlap with excitation band of **1**. Therefore, the

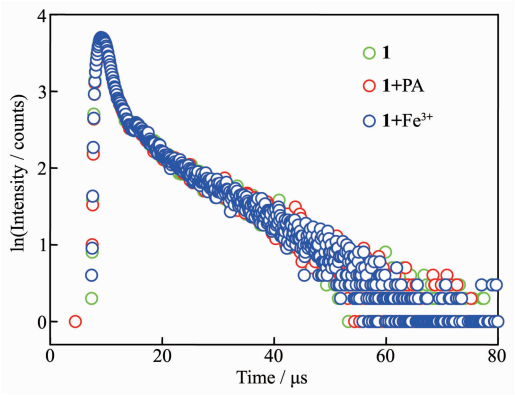

Fig.6　Fluorescence lifetimes of **1** in the absence and presence of PA and Fe^{3+}

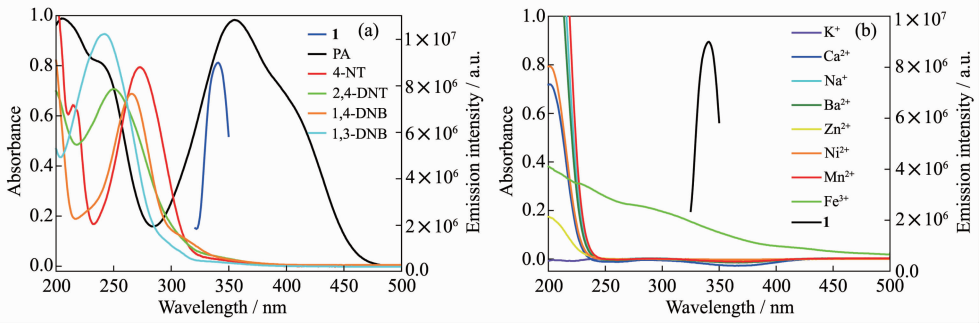

Fig.7　Excitation spectrum of **1** and UV-Vis absorption spectra of different nitroaromatic compounds and metal ions in ethanol solution

luminescence quenching of **1** by PA and Fe^{3+} results from the competition absorption of **1** and PA/Fe^{3+} towards the light source energy.

3　Conclusions

A fishbone-shaped layered coordination polymer with distorted Cd^{2+} octahedra extended by three-connected 2,3-quinoline dicarboxylate linkers was hydrothermally synthesized. More importantly, the highly robust complex emited bright blue fluorescence and can quickly detect the trace amounts of 2,4,6-trinitrophenol and Fe^{3+} through fluorescence quenching with high quenching constants and low limits of detection. Additionally, **1** can be easily regenerated and repeatedly recycled, ensuring its feasible application as a dual-responsive luminescence probe.

Supporting information is available at http://www.wjhxxb.cn

References:

[1] Kreno L E, Leong K, Farha O K, et al. *Chem. Rev.*, **2012**, **112**(2):1105-1125

[2] Lin Y N, Zhang X P, Chen W J, et al. *Inorg. Chem.*, **2017**, **56**(19):11768-11778

[3] Wang B, Lv X L, Feng D W, et al. *J. Am. Chem. Soc.*, **2016**, **138**(19):6204-6216

[4] Zhao D, Liu X H, Zhao Y, et al. *J. Mater. Chem. A*, **2017**,**5**(30):15797-15807

[5] Wu Y L, Yang G P, Zhou X, et al. *Dalton Trans.*, **2015**,**44**(22):10385-10391

[6] Singha D K, Mahata P. *Inorg. Chem.*, **2015**,**54**(13):6373-6379

[7] Gupta A K, Tomar K, Bharadwaj P K. *New J. Chem.*, **2017**, **41**(23):14505-14515

[8] Sathish V, Ramdass A, Velayudham M, et al. *Dalton Trans.*, **2017**,**46**(48):16738-16769

[9] XU Han(徐涵), PAN Zhao-Rui(潘兆瑞). *Chinese J. Inorg. Chem.*(无机化学学报), **2018**,**34**(1):55-62

[9] Hu Y L, Ding M L, Liu X Q, et al. *Chem. Commun.*, **2016**, **52**(33):5734-5737

[10]Hu Z C, Deibert B J, Li J. *Chem. Soc. Rev.*, **2014**,**43**(16):5815-5840

[11]Xiang Z H, Fang C Q, Leng S H, et al. *J. Mater. Chem. A*, **2014**,**2**(21):7662-7665

[12]Ma A Q, Wu J, Han Y T, et al. *Dalton Trans.*, **2018**,**47**(29):9627-9633

[13]Wu Z F, Huang X Y. *Dalton Trans.*, **2017**,**46**(37):12597-12604

[14]Sheldrick G M. *SADABS*, University of Göttingen, Germany, **1996**.

[15]Bruker AXS. *SAINT Software Reference Manual*. Madison: WI, **1998**.

[16](a)Sheldrick G M. *SHELXL*-97, *Program for X-ray Crystal Structure Refinement*, Göttingen University, Germany,**1997**.

(b)Sheldrick G M. *SHELXS*-97, *Program for X-ray Crystal Structure Solution*, Göttingen University, Göttingen, Germany, **1997**.

[17]ZHAO Hong-Kun(赵红昆), DING Bo(丁波), WANG Xiu-Guang(王修光), et al. *Chinese J. Inorg. Chem.*(无机化学学报), **2018**,**34**(9):1739-1746

[18]Deng Q L, Li Y L, Wu J H, et al. *Chem. Commun.*, **2012**,**48**(24):3009-3011